15TH IEA HEAT PUMP CONFERENCE
MAY 26–29, 2026 | HOFBURG VIENNA 2026
DECARBONISATION THROUGH INNOVATION

Experimental investigation of the operating pressure of an ammonia/water absorption heat transformer

Luisa Haak, Louis Tafelmaier, Johannes Brunder,
Konstantinos Stergiaropoulos, Simon Klink

Institute for Building Energetics, Thermotechnology and Energy Storage,
University of Stuttgart, Pfaffenwaldring 6, 70569 Stuttgart, Germany

Abstract

Absorption heat transformers (AHT) are thermal energy converters that elevate heat from a medium to a higher, usable temperature level. To achieve this, some of the heat is dissipated at a lower temperature. The driving energy is primarily supplied as heat at the medium temperature level, while the requirement for electrical energy remains minimal. Therefore, AHT can serve as an alternative to high-temperature compression heat pumps. In this context, they represent a promising technology for decarbonizing the heat generation of industrial processes.
While various working pairs have been studied, research on ammonia/water (NH_3/H_2O) AHT remains limited. Only a few experimental setups have been documented in the literature. This study presents experimental results obtained from a laboratory-scale NH_3/H_2O AHT, delivering heat at temperatures up to 120 °C. The AHT features a continuously adjustable expansion valve, allowing for precise control of the high-pressure level during operation.
This study examined the relationship between internal process variables and system pressure levels. One significant drawback often associated with the NH_3/H_2O working pair is its high operating pressure. However, this study demonstrates that the actual high-pressure level is considerably lower than that predicted by several simulation studies. It is shown that widespread modeling approaches overestimate the pressure requirements of AHT in practical applications and, therefore, limit perceived feasibility. In addition, the influence of the high-pressure level on both useful heat output and COP was analyzed. It is shown that both performance parameters peak at similar high-pressure levels for each operating point. A useful heat output of up to 7.6 kW with a COP of up to 0.37 was achieved at a temperature lift of 30 K.

Selection and/or peer-review under the responsibility of the organizers of the 15th IEA Heat Pump Conference 2026.

Keywords: Absorption heat transformer; Ammonia/water (NH_3/H_2O); High-pressure control; Industrial heat decarbonization; Experimental study

1. Introduction

The ongoing reliance on fossil energy sources remains one of the major challenges in mitigating climate change. In the European Union, the industrial sector is responsible for approximately 20% of total CO_2 emissions. A major contributor is the supply of process heat, which accounts for about 78% and is still generated by fossil fuels. Process heat represents around 66% of the total industrial energy demand. [1] A key pathway for the decarbonization of industrial process heat is electrification. By replacing fossil-fuel-based systems with electric technologies, such as high-temperature compression heat pumps or mechanical vapor recompression, significant reductions in CO_2 emissions can be achieved. However, large-scale electrification also increases electricity demand in general as well as peak loads, which already strain existing distribution and transmission networks. As grid expansion in Germany and other European countries lags behind political and industrial targets, this challenge is expected to intensify in the coming years [2,3].

Against this background, absorption heat transformers (AHT) represent a promising complementary technology. These thermally driven heat pumps upgrade waste heat from a medium temperature (typically 70-100 °C) to a higher useful temperature (around 90-120 °C), while a part of the supplied heat is rejected at a lower temperature. In contrast to compression heat pumps, the required electrical power input accounts for only a few percent of the delivered useful heat. Consequently, AHT offer a viable pathway to upgrade waste

heat and decarbonize industrial heat – especially in an energy system increasingly constrained by grid capacity and rising electricity demand.

Similar to an absorption heat pump or absorption refrigeration processes, an AHT process is based on a binary mixture, referred to as the working pair, composed of a refrigerant and a solvent. The predominant working pair for AHT processes is water/lithium bromide (H_2O/LiBr). This working pair provides high coefficients of performance (COP) but also shows several significant drawbacks such as corrosion issues and the risk of crystallization. Furthermore, since H_2O/LiBr AHT operate under sub-atmospheric pressure, non-condensable gases may enter, which results in a decreased useful heat output and a lower COP. [4,6]

The working pair of ammonia/water (NH_3/H_2O) is less corrosive than H_2O/LiBr, and it overcomes the drawbacks of crystallization and sub-atmospheric pressure. In contrast, it is associated with high operating pressure. The simulation study conducted in [7] indicated the maximum system pressures above 30 bar for a driving temperature of 70 °C and above 50 bar and for a driving temperature 90 °C. Generally, the COP for NH_3/H_2O AHT is lower than that for H_2O/LiBr AHT [7-8]. However, for many industrial applications, the useful heat output is more relevant than the COP itself. By exploiting a larger temperature span on the heat-source side, a simulation study [9] showed that a NH_3/H_2O AHT can cool down the waste heat stream further and thus take up more driving heat. The additional recovered heat could more than compensate for the lower COP, so that the useful heat output of an NH_3/H_2O AHT became comparable to or even higher than that of an H_2O/LiBr AHT for a given heat source [9].

Despite these facts, only limited research on NH_3/H_2O AHT has been reported, and the existing studies are almost exclusively simulation-based, e.g. [7-16]. To the authors' knowledge, only four experimental setups of NH_3/H_2O AHT have been documented in the open scientific literature to date. First, [17] demonstrated the feasibility of the process, achieving useful temperatures >100 °C. Furthermore, [18] showed that upgrading low-grade heat of 60…64 °C was possible without a rectifier, a component that is commonly required for NH_3/H_2O systems. They achieved a thermal COP in the range of 0.400…0.475. In contrast, [19] integrated a rectifier to generate steam below 120 °C while using an 85 °C heat source. In the authors' previous work [20] a NH_3/H_2O AHT built of commercial plate heat exchangers was presented. This AHT was designed for operating pressures up to 40 bar, achieving useful temperatures >115 °C with a driving temperature of 90 °C. The work of [20] revealed a significant deviation between the experimentally observed high-pressure level (< 34 bar) and the high-pressure level predicted from [7] (46 bar) for comparable internal temperatures (absorber: 110 °C; evaporator: 85 °C; condenser: 30 °C). These findings motivated this study, which aims to systematically investigate the high-pressure behavior of NH_3/H_2O AHT.

First, this paper reviews modeling approaches for the high-pressure level of NH_3/H_2O AHT adopted in the literature. To critically evaluate the underlying assumptions, experiments were conducted on a laboratory-scale NH_3/H_2O AHT. The high-pressure level was varied at three different operating points (OP) by using an adjustable expansion valve. The assumptions most commonly used in AHT simulations are applied to estimate the high-pressure level at the OP investigated and compared to the measured values. Furthermore, the influence of the high-pressure level on the achieved heat output and the COP is analyzed.

2. Modeling Approaches for Pressure Levels in NH_3/H_2O Absorption Heat Transformers (AHT)

A closer review of the existing literature shows that most simulation-based studies on AHT using NH_3/H_2O adopt substantial simplifications. The key modeling assumptions are listed in Table 1.

Early works in the 1980s [8,10-12] focused exclusively on internal process temperatures and assumed that pure NH_3 entered the condenser and evaporator. This implied the rectification of the desorbed refrigerant vapor. Consequently, since the refrigerant left the condenser as a saturated liquid and the evaporator as a saturated vapor, the pressure levels directly corresponded to the vapor pressure of NH_3. Therefore, as an example, an evaporator temperature of 85 °C would have resulted in a high-pressure level of approximately 46 bar. This modeling approach was resumed in 2001 in [13] for a comparison of the working pairs NH_3/H_2O and H_2O/LiBr.

In [13], it was assumed that the refrigerant consisted solely of 99 % NH_3, while the assumptions regarding saturation at the outlets of the condenser and evaporator were retained. This indicates that the high pressure at an evaporator temperature of 85 °C would decrease to approximately 21 bar, which is significantly below the saturation pressure of pure NH_3. The study reported in [13] was unique in considering pressure drops between the generator and the condenser, as well as between the evaporator and the absorber. No verification with existing AHT simulations or experimental data was provided.

When modeling an ejector-assisted AHT, the authors of [20] also excluded partial evaporation, calculating the NH_3 concentration based on saturation conditions at the generator outlet.

Recent numerical AHT models became more complex. The first model calibrated against experimental data was presented in [15]. In contrast to most approaches in the earlier literature, this work abandoned the two common assumptions of a saturated-vapor state at the evaporator outlet and a saturated-liquid state at the absorber outlet. This allowed for incomplete evaporation when the refrigerant is non-pure and permitted solution subcooling or vapor carry-under into the solution stream. The high-pressure level was related to the external temperature levels by empirical correlations that are not further defined.

The studies [9] and [16] accounted for the heat transfer to the heat source or sink, defining a pinch point of 5 K in each heat exchanger. They assumed saturated liquid and/or saturated vapor at the outlets of the generator, condenser, and absorber, but did not specify any conditions for the evaporator. The procedure for determining the high-pressure level was not explicitly stated and cannot be unambiguously reconstructed from the published information. In [16], the following conclusions were drawn concerning the system pressure: "The pressures in the machine depends on the cold and waste heat temperature couple values. […] For the highest temperatures, the pressures couple can reach up to 13.5 and 33.5 bars absolute."

Overall, the presented review suggests that pressure levels were often based on simplified and sometimes conflicting assumptions about refrigerant purity, outlet saturation conditions, and pressure drops. Additionally, experimental calibration is limited, and empirical correlations are not well disclosed.

Table 1. Review of assumptions for modeling the high-pressure level of AHT

Authors	Source	Working pair	Type of AHT	Assumption
Stephan & Seher (1984)	[10]	H_2O/LiBr, NH_3/H_2O	single stage / multistage	Saturated vapor of pure NH_3 (H_2O) at evaporator outlet
Ziegler & Alefeld (1987)	[8]	H_2O/LiBr, NH_3/H_2O	single stage / multistage	Saturated vapor of pure NH_3 (H_2O) at evaporator outlet
Tyagi (1987)	[12]	NH_3/H_2O	single stage / multistage	Saturated vapor of pure NH_3 at evaporator outlet
Best et al. (1987)	[11]	NH_3/H_2O	single stage	Saturated vapor of pure NH_3 at evaporator outlet
Ismail (1995)	[13]	NH_3/H_2O	single stage	Saturated vapor of 99 % NH_3 at evaporator outlet pressure drop evaporator–absorber and generator–condenser considered
Kurem & Horuz (2001)	[7]	H_2O/LiBr, NH_3/H_2O	single stage	Saturated vapor of pure NH_3 at evaporator outlet (not explicitly mentioned, but based on Best & Tyagi)
Sözen (2007)	[14]	NH_3/H_2O	single stage with ejector	(Saturated?) vapor at evaporator outlet, NH_3 concentration of refrigerant according to saturation condition at generator outlet
Garone et al. (2017)	[15]	NH_3/H_2O	single stage without rectification	Empirical correlations provide high-pressure level (non-pure refrigerant, incomplete evaporation, no saturation condition at absorber outlet)
Liu et al. (2023)	[9]	NH_3/H_2O	single stage with rectification	"Refrigerant is saturated at outlet of the generator and condenser", no information on state of evaporator outlet
Collignon et al. (2025)	[16]	NH_3/H_2O	single stage without rectification	"Solution is saturated at the outlet of desorber, absorber and condenser" – no information on state of evaporator outlet

3. Experimental Setup

3.1. Process description

Figure 1 shows the flow scheme of the experimental NH_3/H_2O AHT. The process consists of a single-stage cycle with internal heat recovery via solution and refrigerant heat exchangers. No rectifier is implemented. In the generator (13→14), the heat flow $\dot{Q}_{gen}$ is supplied at a low-pressure level to expel the refrigerant from the rich solution, leaving a poor solution. The resulting two-phase mixture enters the separator, where vapor and liquid are separated. The refrigerant is then completely liquefied in the condenser (2→3). The corresponding heat flow $\dot{Q}_{cond}$ is rejected at a low temperature level. The liquid refrigerant enters the refrigerant reservoir, which serves as the refrigerant pump's supply tank. The liquid refrigerant is pumped to the high-pressure level (5→6), preheated in the refrigerant heat exchanger (RHX), (6→7), and then fed into the evaporator. Evaporation takes place at a medium temperature level (7→8). In the absorber, the refrigerant

and the poor solution are mixed (8+18→9). The temperature rises due to absorption. The heat flow $\dot{Q}_{abs}$ released at a high temperature level represents the useful heat output. The rich solution then flows via the solvent reservoir and the first solution heat exchanger (SHX1) to the expansion valve (9→10→11). Expansion at the low-pressure level causes partial evaporation of the rich solution, lowering its temperature. The rich solution is preheated in a second solution heat exchanger (SHX2), (12→13), before flowing into the generator. The poor solution available after desorption is sucked out of the separator and pumped to the absorber via the SHX2 (15→16) and SHX1 (17→18), thus closing the cycle.

The evaporator and generator are arranged in series, with the external heat transfer fluid entering the evaporator first. All external circuits used water as a heat transfer medium. The set pressure prevented evaporation over the studied temperature range up to 120 °C.

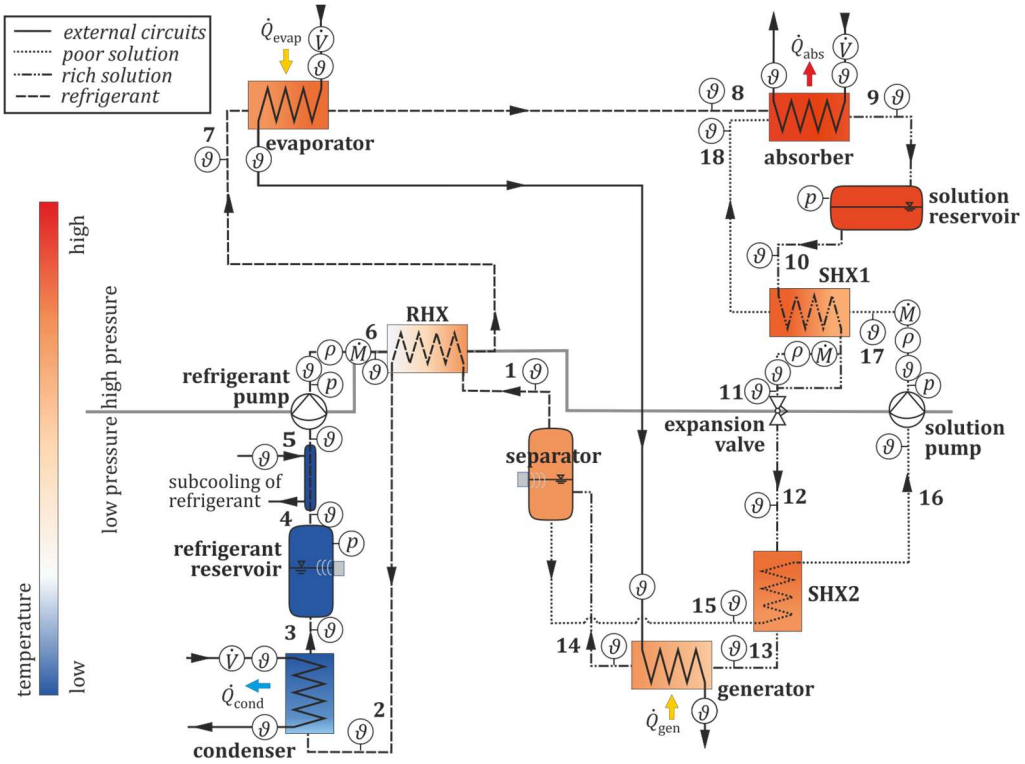

Figure 1. Schematic of the experimental NH_3/H_2O AHT, including instrumentation

3.2. Main components

The presented AHT was designed for a useful heat output of up to 10 kW. All components were rated for a maximum system pressure of 40 bar. Only stainless-steel components were used. A list of supplementary information on the main components is provided in Table 5 in the appendix. Heat exchangers, reservoirs and piping were insulated.

3.2.1. Pumps & expansion valve

Piston-diaphragm pumps of the Verderbar Hydracell G03EKSJHFEMA (Verder) type were used for pumping the refrigerant and the solution. These pumps have three offset pistons, resulting in only minor flow pulsation; and the delivered volume flow is mainly independent of the applied pressure difference. In previous work [20], cavitation-induced instabilities were observed. To mitigate cavitation, both the refrigerant and the weak solution were subcooled at the suction side of the respective pumps. An external thermostat cooled the refrigerant, while the weak solution was cooled by internal heat recovery using an additional SHX, i.e., SHX2. This arrangement not only suppressed cavitation but also lowered the solution pump's operating temperature. [20] A proportional electronic expansion valve (E2V24, Carel) served as the solution throttling valve.

3.2.2. Heat exchangers

All heat exchangers, except for the SHX2, were commercial plate heat exchangers from the AlfaNova HP 27 series (Alfa Laval) with a hard plate corrugation. The generator, absorber, evaporator, and SHX1 were configured as three-pass plate heat exchangers. While the condenser channels were oriented vertically, with

the refrigerant flowing downward due to gravity, all other heat exchangers were installed horizontally. The poor solution was distributed in the absorber via a full-cone spray nozzle; the absorber design is described in detail in [21].

3.3. Instrumentation and data acquisition

Temperatures in the external circuits were measured using Pt100 resistance temperature sensors (tolerance class 1/10 B, calibrated) that were inserted into the flow. External volume flows were measured by electromagnetic flow meters (calibrated). The temperatures of the poor solution and the refrigerant entering the absorber (18 & 8, refer to Figure 1), as well as the rich solution leaving the absorber (9), were measured with in-line Pt100 resistance temperature sensors (tolerance class A, calibrated). Additional internal temperatures were recorded using surface-mounted sensors on piping (Pt100, tolerance class 1/3 B).

The high-pressure level was monitored at three locations: directly downstream of the refrigerant pump, downstream of the solution pump, and at the solution reservoir. On the low-pressure side, the pressure was measured at the refrigerant reservoir.

Coriolis mass flow meters were installed downstream of the refrigerant and solution pumps to measure the respective mass flows and fluid densities. A third Coriolis mass flow meter measured the density of the subcooled rich solution. It was installed on a bypass line so that only a small slipstream of the total rich-solution flow passed through the meter. The bypass flow rate was kept low to limit the pressure drop and therefore prevent flashing. The fluid temperatures directly upstream of the Coriolis meters were measured using Pt100 sensors (tolerance class 1/3 B) in thermowells. For subcooled liquid states, the measured temperature, pressure, and density enable the determination of the corresponding NH_3 mass fraction with an equation of state.

Non-intrusive ultrasonic level switches were mounted on the separator and the refrigerant reservoir and provide binary signals for level control and pump operation.

Control tasks were performed by a Modbus-TCP fieldbus coupler (WAGO 750-362), which also acquired the internal pressure and mass flow signals as well as the state of the level switches. These values were logged every 2 seconds. All other analogue signals were recorded every 4 seconds using Agilent/Keysight 34972A multifunction switch/measure units.

The measurement uncertainties are listed in Table 2. Uncertainties of calculated process variables were obtained using GUM-based uncertainty propagation (expanded uncertainty, k = 2).

Table 2. Measurement uncertainties

Quantity	Instrument	Range	Uncertainty	Comment
Internal temperatures (excl. 8, 9, 18)	Pt100 (surface mounted)		± (1/3 · (0,3 + 0,005 °C^{-1} · ϑ) + 0,15) K	Manufacturer specification
Internal temperatures 8, 9, 18 (inlet, outlet absorber)	Pt100 (in flow)	10…130 °C	± 0.08 K	Calibrated
External temperatures	Pt100 (in flow)	10…130 °C	± 0.08 K	Calibrated
Temperatures at Coriolis mass flow meters	Pt100 (in thermowells)		± (1/3 · (0,3 + 0,005 °C^{-1} · ϑ) + 0,15) K	Manufacturer specification
Pressure (high-pressure side, ref. pump, sol. pump, sol. reservoir)	Pressure transmitter	0…40 bar	± 0.11 bar	Combined expanded uncertainty (k = 2)
Pressure (low-pressure side)	Pressure transmitter	0…17,5 bar	± 0.08 bar	Combined expanded uncertainty (k = 2)
External volumetric flow rate absorber	Electromagnetic flow meter	500…2500 l/h	±0.02 · $\dot{M}$	Calibrated
External volumetric flow rate condenser, evaporator + generator	Electromagnetic flow meter	500…2500 l/h	±0.01 · $\dot{M}$	Manufacturer specification
Internal mass flow rates	Coriolis mass flow meter	0…250 kg/h	±0.001 · $\dot{M}$	Combined expanded uncertainty (k = 2)
Internal densities	Coriolis mass flow meter	0…1000 kg/m^3	± 0.5 kg m^{-3}	Manufacturer specification
Heat flow rate $\dot{Q}_{abs}$	Calculated	2…9 kW	<±6.6 %; (mean < ±3.1 %)	k = 2
Heat flow rate $\dot{Q}_{evap}$+$\dot{Q}_{gen}$	Calculated	14…22 kW	< ± 2.1 %	k = 2
$COP = \dot{Q}_{abs}/(\dot{Q}_{evap}+\dot{Q}_{gen})$	Calculated		< ± 6.9 %	k = 2

4. Testing Procedure

For all experiments, the AHT was charged with 9.8 kg of a NH_3/H_2O solution containing approximately 0.67 NH_3 by mass. The tested operating points (OP) are outlined in Table 3. A thermostatic unit maintained the evaporator inlet temperature. The heat rejected at the condenser was transferred to the building's cooling system, while the heat released at the absorber was dissipated through a dry cooler. In both sink circuits, the target inlet temperatures were controlled by mixing return and bypass streams. The external volumetric flow rates were kept constant: 1000 l/h at the absorber, 2000 l/h in the evaporator-generator circuit, and 2000 l/h at the condenser.

Table 3. Operating points

	Useful temperature level / Absorber outlet ($\vartheta_{ext,abs,out}$)	Driving temperature level / Evaporator inlet ($\vartheta_{ext,evap,in}$)	Cooling temperature level Condenser inlet ($\vartheta_{ext,cond,in}$)
Operating point 1 (OP1)	100 °C	80 °C	25 °C
Operating point 2 (OP2)	110 °C	80 °C	25 °C
Operating point 3 (OP3)	120 °C	90 °C	25 °C

The solution pump was operated with a level-based control strategy to maintain a constant filling level in the respective reservoirs. A non-intrusive ultrasonic level switch, which was installed at a medium height of the reservoir, provided a binary signal indicating whether liquid is present at the sensor position. If fluid was detected, the pump's speed was increased in small steps. In case the fluid level was below the sensor position, the pump's speed was decreased in small steps. As a result, the poor solution mass flow rate exhibited a periodic, triangular-wave-like variation around its mean values. This control strategy ensured a continuous supply of liquid to the pump but introduced small periodic fluctuations in the supplied and rejected heat flows as well as in the temperatures of the external circuits. The refrigerant pump was controlled equally at OP3. At OP1 and OP2, the refrigerant reservoir's filling level did not reach the level switch's height. Therefore, the refrigerant pump was set to its minimum speed, what led to a constant refrigerant mass flow. The refrigerant was cooled at the suction side of the refrigerant pump to prevent cavitation.

For each OP, the opening degree of the electronic expansion valve was systematically varied to adjust the high-pressure level. After reaching stable operation for a valve setting, data were recorded for 30 min and time-averaged values were calculated.

The equation of state by Tiller-Roth and Friend [22] was used to calculate the NH_3 mass fraction of the refrigerant, the poor, and the rich solution from the corresponding measured temperatures, pressures, and densities. Further thermodynamic properties can thus be calculated for every state point. The thermodynamic properties of water required for the energy balances of the external circuits were calculated with CoolProp [23].

As discussed in Section 2, the pressure levels in many simulation studies were fixed by assuming the refrigerant was saturated liquid at the condenser outlet and saturated vapor at the evaporator outlet. Furthermore, the refrigerant NH_3 mass fraction was considered to be $\xi_{ref} = 1$. To enable comparison with these assumptions, the corresponding refrigerant temperatures were estimated using a fixed pinch point of $\Delta\vartheta_{pin}$ = 5 K between the refrigerant and the external fluid in the condenser and evaporator, following [9], [16]. The resulting pressures are listed in Table 4. Since OP1 and OP2 share the same driving temperature, they are expected to have an identical evaporation pressure and, consequently, an identical high-pressure level. In contrast, OP3 is predicted to have a pressure level 9 bar higher than OP1 and OP2.

Table 4. Condensation and evaporation pressures derived from simulation assumptions for operating points OP1-OP3

	Condensation temperature $\vartheta_{ref,cond,out} \approx \vartheta_{ext,cond,in} + \Delta\vartheta_{pinch}$	Condensation pressure $p_{sat}(\xi_{ref}=1, \vartheta_{ref,cond,out})$	Evaporation temperature $\vartheta_{ref,evap,out} \approx \vartheta_{ext,evap,in} - \Delta\vartheta_{pinch}$	Evaporation pressure $p_{sat}(\xi_{ref}=1, \vartheta_{ref,evap,out})$
OP1	30 °C	11.7 bar	75 °C	37.1 bar
OP2	30 °C	11.7 bar	75 °C	37.1 bar
OP3	30 °C	11.7 bar	85 °C	46.1 bar

5. Results and Discussion

5.1. Variation of high-pressure level

5.1.1. Effect of expansion valve opening on pressure levels

Figure 2 shows the influence of the expansion valve opening on the pressure levels (a), on the mass flow rate of the poor solution and the refrigerant (b), the NH_3 mass fraction of the refrigerant (c) and the vapor quality at the evaporator outlet (d) for the three OP. The abscissa shows the control voltage of the expansion valve U_{EV}. The expansion valve's near-proportional behavior allows the control voltage to serve as a surrogate for valve opening in the presented plots, with the valve fully closed at 0 V and fully open at 10 V. The high-pressure values provided in Figure 2(a) correspond to the pressure measured at the solution reservoir, which is considered representative of the pressure at the absorber and the evaporator. (The pressure drop from the evaporator across the piping and the absorber to the measuring point at the solution reservoir was estimated to < 500 mbar). The higher pressures observed directly downstream of the solution pump were influenced by the pressure drop across the Coriolis mass flow meter. Therefore, these values were unsuitable for comparison with simulation results based on thermodynamic equilibrium states. The maximum local pressure, which is relevant for practical application, was found on the discharge side of the solution pump. For the AHT studied, it was elevated by 1 to 2 bar due to the connecting piping, the solution heat exchanger, and the distribution nozzle.

The pressure values derived from the simulation assumptions (see Table 4) are shown as dashed lines. This enables us to critically evaluate those assumptions.

On the low-pressure side, the measured pressure remained nearly constant across all OP and valve openings, closely matching the saturation pressure of NH_3, 11.7 bar, at the estimated condensation temperature. Therefore, assuming a saturated liquid at the condenser outlet is justified.

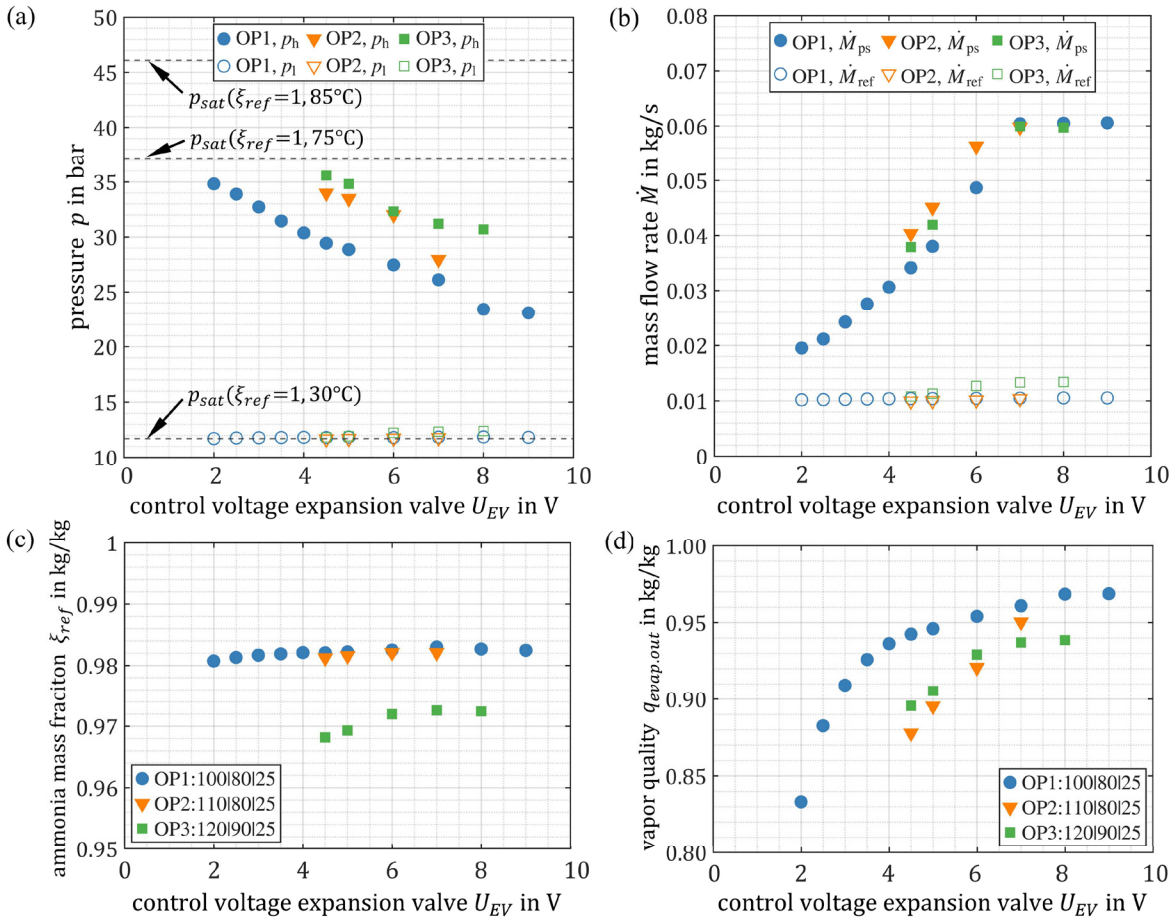

Figure 2. Influence of valve opening on (a) pressure levels, (b) mass flow rates of poor solution and refrigerant, (c) NH_3 mass fraction of the refrigerant, and (d) vapor quality at the evaporator outlet for the three OP. Dashed lines in (a) indicate the saturation pressure of NH_3 ($\xi_{ref} = 1$) at the assumed condensation and evaporation temperatures used in simulation studies.

In contrast, the high-pressure level decreased as the valve opening increases. The highest pressure value of p_h = 35.6 bar was reached for OP3 at U_{EV} = 4,5 V. For both OP2 and OP3 the maximum system pressure would have been exceeded at lower valve opening. When comparing identical valve openings, the high-pressure levels measured at OP2 were up to 4.5 bar higher than those at OP1. Since OP1 and OP2 have the same driving temperature, this does not support the assumption that the saturation condition at the evaporator outlet determines the high-pressure level. In contrast, the observed difference in the high-pressure level of OP1 and OP2 suggests a possible influence of the useful temperature level. In general, the measured high-pressure levels remained significantly below the saturation pressure of pure NH_3 at the evaporator outlet temperature.

Figure 2(b) displays the mass flow rates of refrigerant and poor solution. The refrigerant mass flow rate $\dot{M}_{ref}$, which is shown as unfilled symbols, varied only slightly with valve opening for all OP. In contrast, the poor solution mass flow rate $\dot{M}_{ps}$ gradually rose with increasing U_{EV} as a higher pump speed was required to maintain a constant level in the separator. At valve openings corresponding to $U_{EV} \geq 7$ V, the poor-solution mass flow of the poor solution reached a plateau determined by the maximum volume flow rate of the solution pump. For OP1, stable operation was achieved over a wide range of valve openings (2 V $\leq U_{EV} \leq$ 9 V). At higher openings, the pump could not prevent the flooding of the separator, whereas the minimum pump speed was reached at U_{EV} = 2 V. It can be concluded that varying the valve opening requires adjusting the solution pump speed.

To further examine the deviation of simulated and measured pressure levels, the Figure 2(c) and (d) present the corresponding NH_3 mass fraction and vapor quality at the evaporator outlet. The refrigerant NH_3 mass fraction for OP1 and OP2 ranged from 0.980 to 0.985. The slightly lower NH_3 mass fraction of approximately 0.97 can be attributed to the higher driving temperature and, consequently, a higher generator temperature, which results in a lower NH_3 mass fraction in the desorbed refrigerant vapor.

As shown in Figure 2(d), the vapor quality at the evaporator outlet rose as the valve opening increased. For OP1, the vapor quality ranged from 0.83 to a maximum of 0.97. At corresponding valve openings, OP2, with the same driving temperature as OP1, showed lower vapor qualities than OP1. Both observations can be attributed to increasing pressure. OP3 tended to have higher vapor qualities than OP2 at similar pressures, due to the higher driving temperature of OP3.

The assumptions of pure NH_3 and complete evaporation were unlikely to be met here, since no rectifier was used. From a practical perspective, it remains to be assessed whether the additional technical effort of employing a rectifier to increase refrigerant purity to ξ_{ref} = 1.0 is justified, particularly because higher purity would be expected to increase the system pressure.

According to the literature on absorption chillers and heat pumps, impurities cause the refrigerant to exhibit a strong temperature glide, making complete evaporation difficult [24]. Therefore, the approach of assuming an impure refrigerant (ξ_{ref} = 0.99 / saturated vapor at generator outlet) but still applying complete evaporation as done in [13] and [14] is also questionable. An alternative, but still straightforward approach for very simple AHT simulations could be to set the vapor quality at the evaporator outlet to a fixed value, as done in [24] for modeling an absorption chiller.

5.1.2. Internal state analysis

Figure 3(a) shows selected internal state points for all three OP at an control voltage of the expansion valve of U_{EV} = 5 V in a Dühring plot. In this plot, the saturation pressure is plotted on a logarithmic scale against the negative reciprocal of the saturation temperature, yielding approximately linear behavior for NH_3/H_2O mixtures at constant composition. Since the diagram is based on saturation properties, only to state points that can be approximated as saturated liquid are plotted.

The condition of saturated liquid was achieved in good approximation at the condenser outlet (3) and the absorber outlet (9) across all three OP at a medium control voltage of the expansion valve, e.g. U_{EV} = 5 V. As it will be shown in Section 5.2, the chosen control voltage of the expansion valve resulted in both a high useful heat output and a high COP for all three OP. The liquid phase at the desorber inlet and outlet is represented by (13) and (14), respectively. Whereas state point (9) indicates the NH_3 mass fraction of the rich solution, state point (14) represents the NH_3 mass fraction of the poor solution. For OP1 and OP2, the NH_3 mass fractions of the poor solution are 0.477 and 0.473, respectively. This difference is within the measurement uncertainty and is therefore not considered significant. For the rich solution, the NH_3 mass fraction differs more noticeably (0.591 in OP1 and 0.572 in OP2). A plausible explanation is the higher absorber temperature, which is expected to lower the solution's capacity to absorb NH_3. For OP3, both rich- and poor-solution NH_3 mass fractions are shifted to lower values compared to OP1 and OP2. This shift is attributed to the higher liquid level in the refrigerant reservoir for OP3 (approximately 10 cm), which reduces the NH_3 mass in the solution loop by about 0.8 kg. Hence, one plausible explanation for the comparatively small increase in high-pressure

level from OP2 to OP3 is the solutions reduced NH_3 mass fraction, which results from the applied control strategy.

Point M was not directly measured and represents the temperature within the cycle calculated as the adiabatic mixing point within the manifold of the absorber. A comparison between the temperature at point M and the absorber outlet temperature of the external fluid, i.e., the useful temperature level, indicates that only a small heat-transfer potential remained within the absorber.

The evaporator inlet (7) might be at subcooled or two-phase state; therefore, the refrigerant's boiling temperature is shown. To complement the Dühring representation Figure 3(b) reports the measured refrigerant's inlet and outlet temperatures at the evaporator separately. The refrigerant's temperature at the evaporator outlet $\vartheta_{ref,evap,out}$ was largely independent of U_{EV} and thus of the high-pressure level. Since the pinch-point temperature difference was only 2…3 K, the assumption of $\Delta\vartheta_{pinch}$ = 5 K used to estimate the pressure levels for comparison with the simulation assumptions (Table 4) can be considered conservative.

Overall, the internal state analyses suggests that the high-pressure level is influenced not only by temperature levels but also by the solution composition, in particular the NH_3 mass fraction of the rich solution. This hypothesis is qualitative and requires further verification. In practice, the NH_3 mass fraction of the rich solution can be affected by adjusting the refrigerant-reservoir level or by the composition and amount of the total system charge.

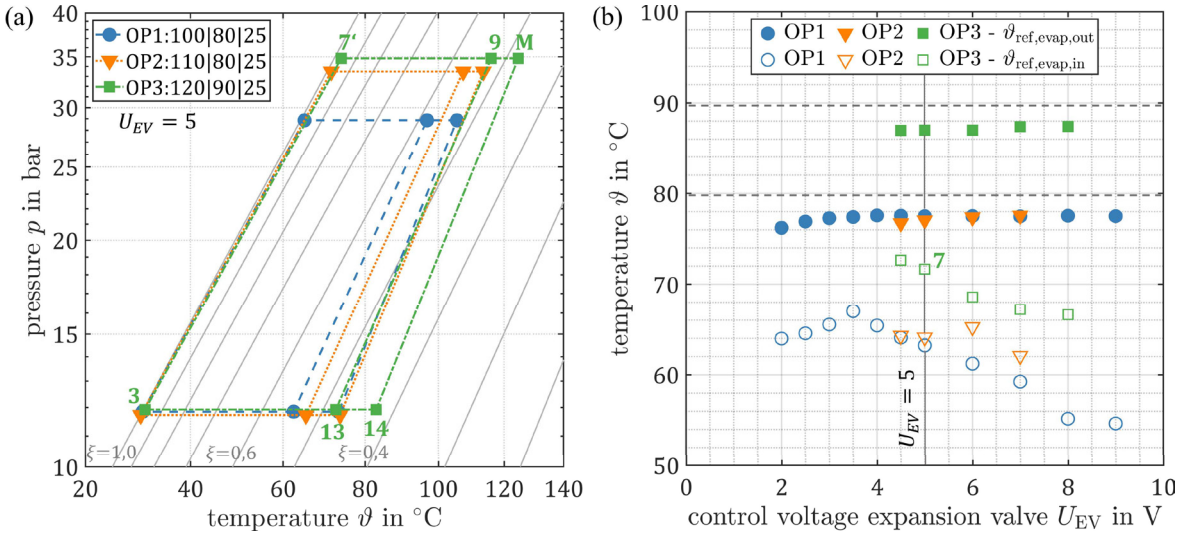

Figure 3. (a) State points of the three OP points at an expansion valve control voltage of U_{EV} = 5 V displayed in a Dühring plot. **3** condenser outlet; **7'** evaporator boiling point; **M**: adiabatic mixing point (calculated); **9** absorber outlet; **13** generator inlet; **14**: generator outlet. (b) Measured refrigerant temperatures at the evaporator inlet and outlet against expansion valve control voltage.

5.2. Influence of high-pressure level on heat output and COP

Next, the influence of the high pressure on the performance of the AHT was evaluated. Figure 4 displays the useful heat output $\dot{Q}_{abs}$, which is discharged at the absorber, (a) and the COP (b) over the high-pressure level. The COP is defined as the ratio of the useful heat output to the driving energy supplied at the evaporator and generator:

$$COP = \dot{Q}_{abs}/(\dot{Q}_{evap} + \dot{Q}_{gen}) \quad (1)$$

OP1 showed the highest useful heat output, peaking at $\dot{Q}_{abs}$ = 8.8 kW in a pressure range of p_h = 27.5…29.4 bar. The COP simultaneously reached 0.41 in this pressure range. Both heat output $\dot{Q}_{abs}$ and COP declined at higher high-pressure levels. At lower high-pressure levels, corresponding to large valve openings ($U_{EV} \geq 8$ V), both quantities, $\dot{Q}_{abs}$ and COP, experienced a sharp drop. A similar behavior was found for OP2. The slightly lower maxima of $\dot{Q}_{abs}$= 6.7 kW and COP = 0.36 were found at comparable valve openings but shifted to a higher high-pressure level. The lower performance was an expected outcome, since OP2 is characterized by a higher temperature lift. OP3 showed the highest heat output $\dot{Q}_{abs}$ and COP at the highest feasible valve openings corresponding to a control voltage of U_{EV} = 4,5…5 V. The COP of OP3 was similar to the COP of OP2, while the useful heat output of $\dot{Q}_{abs}$ = 7.6 kW was higher.

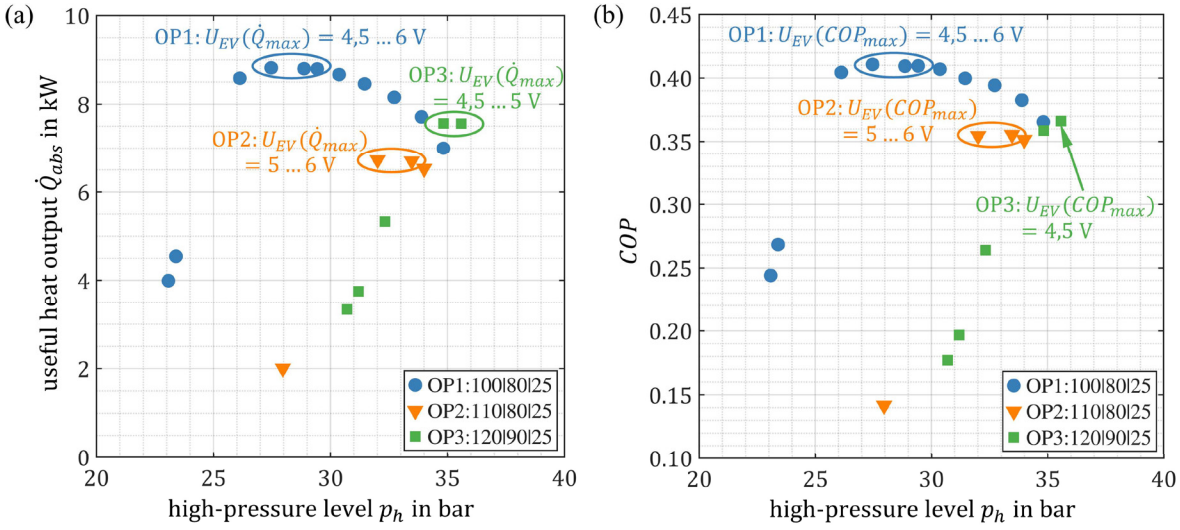

Figure 4. Influence of the high-pressure level on (a) the useful heat output $\dot{Q}_{abs}$ discharged at the absorber and(b) the *COP*.

For high-performance measurement points, the rich solution is a saturated liquid within the scope of measurement uncertainty. In contrast, for lower-performance measurement points at high valve openings, a leap to vapor qualities to $q_{rs,abs,out} \approx 0.1$ was reported. Thus, significantly lower values of $\dot{Q}_{abs}$ and COP observed at all OP are related to incomplete absorption. When designing a control strategy for the expansion valve to optimize the useful heat output and COP, the valve opening should be slightly underestimated rather than overestimated. For the three OP investigated in this study, a fixed throttling device with an opening equivalent to $U_{EV} = 4{,}5$ V would have delivered robust performance. However, it has to be noted that no variation of the temperature of the condenser has been conducted. Expanding the operating area might render the adjustable expansion valve advantageous. Furthermore, an adjustable expansion valve remains beneficial to find the optimal balance between permissible pressure and performance degradation as seen at OP3.

6. Conclusions

Absorption heat transformers (AHT) are thermally driven heat pumps that upgrade waste heat from a medium temperature to a higher useful temperature, while a part of the supplied heat is rejected at a lower temperature. This work focuses on the influencing factors on the operating pressure of an NH_3/H_2O AHT. A review of modeling approaches for the high-pressure level of NH_3/H_2O AHT showed that most simulation studies assumed saturated vapor of pure NH_3 at the evaporator outlet. Consequently, the high-pressure level is related direct to the driving temperature.

To critically assess the assumptions found in the literature, the high-pressure levels were experimentally investigated. The high-pressure level was systematically varied for three different operating points (OP) using an adjustable expansion valve. The following results were obtained:

- By decreasing the valve opening, the high-pressure level increased. As the valve opening decreased, the solution circulation rate decreased, so that the solution pump speed was reduced accordingly.
- Simulations overestimated the AHT's operating pressure. The highest operating pressure of p_h = 35.6 bar was achieved at OP3 (useful temperature level: 120 °C; driving heat: 90 °C; cooling: 25 °C). Using the modeling approaches adopted in the literature would result in an overestimation of the high-pressure level by >10 bar.
- The key assumption of pure NH_3 leaving the evaporator at saturation state does not apply: the experimentally determined NH_3 mass fraction was 0.978…0.985, whereas the vapor quality ranged from 0.83 to a maximum of 0.97. This is because no rectification was used. It remains to be assessed whether the additional effort required for rectification is justified in practical applications, given that higher refrigerant purity would likely be associated with an increased high-pressure level.
- The high-pressure level influences the useful heat output and the COP. Both performance parameters peaked at similar high-pressure levels for each OP.
- A useful heat output of up to 7.6 kW with a COP of up to 0.37 was achieved at a temperature lift of 30 K.

Nomenclature

Variables			*Subscripts*	
COP	coefficient of performance $COP = \dot{Q}_{\text{abs}}/(\dot{Q}_{\text{evap}} + \dot{Q}_{gen})$	−	abs	absorber
			$cond$	condenser
Δp_{pinch}	temperature difference at pinch point	K	ext	external
$\dot{M}$	mass flow rate	kg/s	$evap$	evaporator
p	pressure	bar	gen	generator
$\dot{Q}$	heat flow rate	kW	h	high-pressure level
U_{EV}	control voltage expansion valve	V	l	low-pressure level
$\dot{V}$	volumetric flow rate	l/h	$lift$	(temperature) lift
ϑ	temperature	°C	max	maximum
ξ	ammonia (NH_3) mass fraction	kg/kg	out	outlet
ρ	density	kg/m^3	ps	poor solution
			ref	refrigerant
Acronyms			rs	rich solution
AHT	absorption heat transformer		sat	saturation
H_2O/LiBr	water/lithium bromide (working pair)			
NH_3/H_2O	ammonia/water (working pair)			
OP	operating point			
RHX	refrigerant heat exchanger			
SHX	solution heat exchanger			

Acknowledgements

The laboratory-scale NH_3/H_2O AHT presented in this work was developed in a project (grant number "01IF22424 N") funded by the German Federal Ministry for Economic Affairs and Climate Action.

Appendix

Table 5. Main components of the studied AHT.

Component	Manufacturer, Type	Description
Generator	Alfa Laval, AlfaNova HP 27-64H	Brazed plate heat exchanger, 3-pass, horizontal installation
Absorber	Alfa Laval, AlfaNova HP 27-48H	Brazed plate heat exchanger, 3-pass, horizontal installation; solution distributed by full-cone spray nozzle
Condenser	Alfa Laval, AlfaNova HP 27-40H	Brazed plate heat exchanger, single pass, vertical installation
Evaporator	Alfa Laval, AlfaNova HP 27-48H	Brazed plate heat exchanger, 3-pass, horizontal installation
Refrigerant heat exchanger (RHX)	Alfa Laval, AlfaNova HP 27-22H	Brazed plate heat exchanger, single pass, horizontal installation
Solution heat exchanger, high-pressure side (SHX-HD)	Alfa Laval, AlfaNova HP 27-22H	Brazed plate heat exchanger, 3-pass, horizontal installation
Solution heat exchanger, low-pressure side (SHX-LP)	TTZ, custom asymmetric plate heat exchanger	Single-pass, vertical installation; enlarged flow cross-section on rich-solution side
Solution expansion valve	Carel, E2V24	Electronically controlled expansion valve
Solution pump	Verder / Hydra-Cell G03EDSTHHEMA	Piston-diaphragm pump, max. electrical power 0.55 kW, variable speed
Refrigerant pump	Verder / Hydra-Cell G03EDSTHHEMA	Piston-diaphragm pump, max. electrical power 0.55 kW, variable speed
Absorber nozzle	Lechler, type 490.608	Full-cone spray nozzle, spray angle 120°

References

[1] Boer, R. de, Marina, A., Zühlsdorf, B., Arpagaus, C., Bantle, M., Wilk, V.,Elmegaard, B., Corberan, J., Benson: Strengthening Industrial Heat Pump Innovation: Decarbonizing Industrial Heat, 2020.

[2] Bürger, J.J.: Transformationsprozesse und Stromnetzausbau, *Springer Fachmedien Wiesbaden*, Wiesbaden, Germany, 2018.

[3] Linnemann, J.F.: Quo vadis Stromnetz?, *Springer Fachmedien Wiesbaden*, Wiesbaden, Germany, 2025.

[4] Cudok, F., Giannetti, N., Ciganda, J.L.C., Aoyama, J., Babu, P., Coronas, A., Fujii, T., Inoue, N., Saito, K., Yamaguchi, S., Ziegler, F.: Absorption heat transformer - state-of-the-art of industrial applications, *Renewable and Sustainable Energy Reviews*, vol. 141, p. 110757, 2021.

[5] Rivera, W., Best, R., Cardoso, M.J., Romero, R.J.: A review of absorption heat transformers, *Appl. Therm. Eng.*, vol. 91, pp. 654–670, 2015.

[6] Metzner, D., Corrales Ciganda, J.L.: Einfluss von nicht-kondensierbaren Gasen auf den thermodynamischen Prozess im Absorptionswärmetransformator: Eine experimentelle Untersuchung mit Stickstoff in *Jahrestagung des Deutschen Kälte- und Klimatechnischen Vereins,* Ulm, Germany, 2019.

[7] Kurem E., Horuz I.: A comparison between ammonia-water and water-lithium bromide solutions in absorption heat transformers, *International Communications in Heat and Mass Transfer*, vol. 28, no. 3, pp. 427–438, 2001.

[8] Ziegler, F., Alefeld, G.: Coefficient of performance of multistage absorption cycles, *International Journal of Refrigeration*, vol. 10, no. 5, pp. 285–295, 1987.

[9] Liu, Z., Lu, D., Shen, T., Cheng, R., Chen, R., Gong, M.: Improving heat supply of ammonia-water absorption heat transformer by enlarging heat source utilization temperature span, *Energy*, vol. 280, p. 128219, 2023.

[10] Stephan, K., Seher, D.: Heat transformer cycles—I. One- and two-stage processes, *Journal of Heat Recovery Systems*, vol. 4, no. 5, pp. 365–369, https://www.sciencedirect.com/science/article/pii/0198759384900547, 1984.

[11] Best, R., Eisa, M., Holland, F.A.: Thermodynamic design data for absorption heat transformers—III. Operating on ammonia-water, *Heat Recovery Systems and CHP*, vol. 7, no. 3, pp. 259–272, 1987.

[12] Tyagi, K.P.: Aqua-ammonia heat transformers, *Heat Recovery Systems and CHP*, vol. 7, no. 5, pp. 423–433, 1987.

[13] Ismail, I.: Upgrading of heat through absorption heat transformers, *International Journal of Refrigeration*, vol. 18, no. 7, pp. 439–446, 1995.

[14] Sözen, A.,Yücesu, H.S.: Performance improvement of absorption heat transformer, *Renewable Energy*, vol. 32, no. 2, pp. 267–284, 2007.

[15] Garone, S., Toppi, T., Aprile, M., Motta, M.: A tuned model to optimize a water-ammonia heat transformer in *International Sorption Heat Pump Conference 2017,* Tokyo, 2017.

[16] Collignon, R., Demasles, H., Phan, H.T.: Modeling of an Ammonia/Water Absorption Heat Transformer to upgrade low-temperature industrial waste heat both at machine scale and at local scale inside the falling film absorber, *Thermal Science and Engineering Progress*, vol. 59, p. 103302, 2025.

[17] Mostofizadeh, C.: Theorie und Praxis der Wärmetransformation zur Nutzung von Abfallwärme, Düsseldorf, Germany 1980.

[18] Garone, S., Toppi, T., Guerra, M.,Motta, M.: A water-ammonia heat transformer to upgrade low-temperature waste heat, *Appl. Therm. Eng.*, vol. 127, pp. 748–757, 2017.

[19] Liu, Z.,Lu, D., Tao, S., Chen, R., Gong, M.: Experimental study on using 85 °C low-grade heat to generate <120 °C steam by a temperature-distributed absorption heat transformer, *Energy*, vol. 299, p. 131491, 2024.

[20] Haak, L., Vollmer, A., Brunder, J., Stergiaropoulos, K.: NH3/H2O-Absorptionswärmetransformator: Erhöhung der Betriebsstabilität in *Jahrestagung des Deutschen Kälte- und Klimatechnischen Vereins,* Dresden, Germany, 2024.

[21] Mirl, N.: Analyse und Optimierung einer einstufigen Ammoniak/Wasser-Absorptionswärmepumpe, *Dissertation, Institut für Gebäudeenergetik, Thermotechnik und Energiespeicherung, University of Stuttgart*, Stuttgart, Germany, 2021.

[22] Tillner-Roth, R., Friend, D.G.: A Helmholtz Free Energy Formulation of the Thermodynamic Properties of the Mixture {Water + Ammonia}, *J. Phys. Chem. Ref. Data*, vol. 27, no. 1, pp. 63–96, 1998.

[23] Bell, I.H., Wronski, J., Quoilin, S., Lemort, V.: Pure and Pseudo-pure Fluid Thermophysical Property Evaluation and the Open-Source Thermophysical Property Library CoolProp, *Industrial & engineering chemistry research*, vol. 53, no. 6, pp. 2498–2508, 2014.

[24] Herold, K.E., Radermacher, R., Klein, S.A.: Absorption Chillers and Heat Pumps, *CRC Press*, London, New York, Boca Raton, 2016.